Design and optimization of a kinase-controlled allosteric switch

Qinhao Cao[1], Jared E. Toettcher[1,2]

[1] Department of Molecular Biology, Princeton University, Princeton NJ 08544

[2] Omenn-Darling Bioengineering Institute, Princeton University, Princeton NJ 08544

Correspondence should be addressed to:

Jared Toettcher, toettcher@princeton.edu

Abstract

Post-translational control enables rapid and precise regulation of cell behavior. Despite these advantages, general strategies to build phosphorylation-based synthetic circuits are limited. Here, we reasoned that engineered allostery, a technique that has been applied to design light- and chemically-gated protein switches, could also be used to engineer phosphorylation-controlled protein switches (phospho-switches). Using an allosterically controllable Gal4 transcription factor as a scaffold, we show that a classic kinase FRET biosensor architecture can be used as a starting point for phospho-switch design. We optimize all features of the phospho-switch to develop an ERK-controlled transcription factor with a 20-fold phosphorylation-dependent change in transcriptional output. Our switch outperforms the *c-fos* promoter, a classic ERK-responsive transcriptional biosensor, in selectivity and sensitivity. We further show that our switch architecture can be generalized to other input kinases and allosterically controlled targets. This work provides a general platform for a new generation of kinase-responsive tools for biosensing and synthetic biology applications.

Introduction

Cells rely on protein phosphorylation as a primary carrier of intracellular information. Protein kinases are activated by a variety of stimuli and regulate diverse processes including cytoskeletal assembly, metabolism, protein localization, and gene expression. Phosphorylation can also link multiple kinases and substrates into networks that can perform diverse signal processing capabilities, including signal integration[1], amplification[2], and feedback control[3]. Yet while bioengineers have long been able to build synthetic transcriptional circuits[4,5], our ability to engineer post-translational networks has been far more limited.

Recent studies have already begun to demonstrate the power of synthetic post-translational control for sensing and rewiring oncogenic states, constructing neural networks to perform information processing in cells, and improving engineered cell-based therapies[6–9]. Yet each of these studies relied on engineered protease-substrate interactions to perform stimulus-dependent irreversible cleavage of an effector domain[10,11]. In contrast to protein cleavage, the reversibility of protein phosphorylation presents an opportunity to provide bidirectional control for more fine-tuned responses in space and time. Moreover, synthetic phosphorylation-based logic would make it possible to directly interface with the kinome to sense kinase-encoded cell states and trigger desired responses.

Engineering proteins whose activity is controlled by defined phosphorylation events is challenging, but some studies have begun to address this challenge. A pioneering study demonstrated that a novel phosphorylation site could be introduced into the *Saccharomyces cerevisiae* kinase Kss1 to regulate its activity[12]. Phosphorylation-dependent binding has also been used in *S. cerevisiae* to re-localize cytosolic proteins to the plasma membrane, activating cellular processes in cases where membrane localization is essential for function[13]. Most recently, synthetic phosphorylation relays were constructed in mammalian cells using combinations of engineered tyrosine kinases, phospho-tyrosine (pTyr) peptides, and SH2 pTyr-binding domains[14]. General methods for phosphorylation-dependent control of protein function could power advances in synthetic biology by enabling the production of compact phosphorylation-based intracellular circuits.

Engineered allostery is a powerful concept for achieving stimulus-dependent control over protein function. In engineered allostery, a stimulus-regulated protein domain (switch) is inserted at a particular site in a target protein, such that a conformational change in the switch alters the target protein's function (**Fig. 1A**). Several domains, including the light-sensitive AsLOV2 domain and ligand-responsive uniRapR domain, can act as suitable stimulus-dependent switches, changing conformation in response to illumination or addition of a small molecule (**Fig. 1B**)[15,16]. However, no switches are yet available to respond to protein phosphorylation. A kinase-controlled phosphorylation-dependent switch could immediately confer phospho-regulation to the diverse set of target proteins previously engineered to be controlled by light or small molecule addition.

Here, we discover that a commonly used Förster resonance energy transfer (FRET) kinase biosensor provides a starting point for the development of a kinase-controlled allosteric switch. We show that the EKAR biosensor[17,18] for the Extracellular Signal-Related Kinase (ERK), can function as a prototype kinase-controlled switch when inserted into a Gal4 transcription factor at a previously identified allosteric site. We systematically optimize each component of the switch (hinge, phospho-peptide, and phospho-binding domain) to substantially improve its potency and

dynamic range, revealing design principles for achieving phosphorylation-dependent allostery that differ from FRET biosensors. Our final switch design results in a >20-fold change in transcriptional output between phosphorylated and unphosphorylated states. We show that our synthetic kinase-controlled transcription factor functions as an excellent biosensor of ERK kinase activity, outperforming the FOS promoter in sensitivity and selectivity for ERK over other stimuli. Our switch generalizes to multiple kinases and allosterically-controlled target proteins, including a JNK-controlled transcription factor and an ERK-controlled actin nanobody. Overall, this strategy expands the synthetic biologist's toolbox of post-translationally regulated processes to a diverse suite of kinases and allosterically-controlled target proteins with potential applications in biosensor design, drug screening, and cell-based therapy.

Results

Repurposing FRET-based kinase activity reporters as allosteric switches

Our strategy for achieving kinase-triggered allosteric control requires a phosphorylation-regulated sensory domain (phospho-switch) that can regulate the conformation of a target protein based on the activity of a specific upstream kinase. An ideal phospho-switch would satisfy a few criteria. First, phosphorylation should trigger an open-to-closed conformational change that alters the distance between the switch's N and C termini, in a similar manner to successful chemogenetic and optogenetic allosteric switches[15,16]. Second, it should be rapidly and reversibly regulated by phosphorylation from a defined kinase of interest. Third, the switch design should be modular and generalizable to multiple kinase inputs.

We reasoned that FRET-based kinase activity reporters (KARs) provide an attractive starting point for satisfying each of these criteria. The sensory region in KARs consists of a phosphorylatable substrate, a flexible hinge, and a phosphate-binding domain (phospho-binder)[19]. Binding between the phosphorylated substrate and phospho-binder brings fluorescent proteins on the KAR's N and C termini into proximity to produce a change in fluorescence (**Fig. 1C**). KARs have been shown to rapidly and reversibly report on kinase activity, and due to their modular design, many KARs targeting diverse kinases (e.g., ERK, PKA, SRC) have already been developed and validated[20]. We thus hypothesized that KAR sensory domains could be repurposed as prototype phospho-switches to allosterically control target proteins of interest. We focused on the EKAR-EV biosensor for the ERK kinase, a cell signaling protein that is activated by extracellular growth factors and whose activity stimulates cell growth and differentiation during development, tissue regeneration, and cancer progression. The EKAR-EV biosensor contains an ERK-responsive sensory domain that includes an ERK-phosphorylatable peptide (amino acids PRTP) and docking motif (FQFP), an 88 amino acid Gly/Ser/Ala hinge, and the Pin1 WW phospho-binding domain[17,18].

We chose an engineered transcription factor formed from the Gal4 DNA binding domain and the VP64 transactivation domain as a model target protein for implementing ERK-based allosteric control. In a recent study, we developed a light-controlled Gal4-VP64 variant by inserting the photoswitchable AsLOV2 domain between positions Ser22 and Lys23 (SK22) inside the Gal4 DNA-binding domain (**Fig. 1D**). The resulting OptoGal4 system exhibits potent allosteric control, with a >100-fold change in transcription activity between blue light illumination and dark conditions[21]. We replaced the AsLOV2 module with the EKAR sensory domain to test whether the light-responsive protein could instead be made to sense a change in phosphorylation state, terming

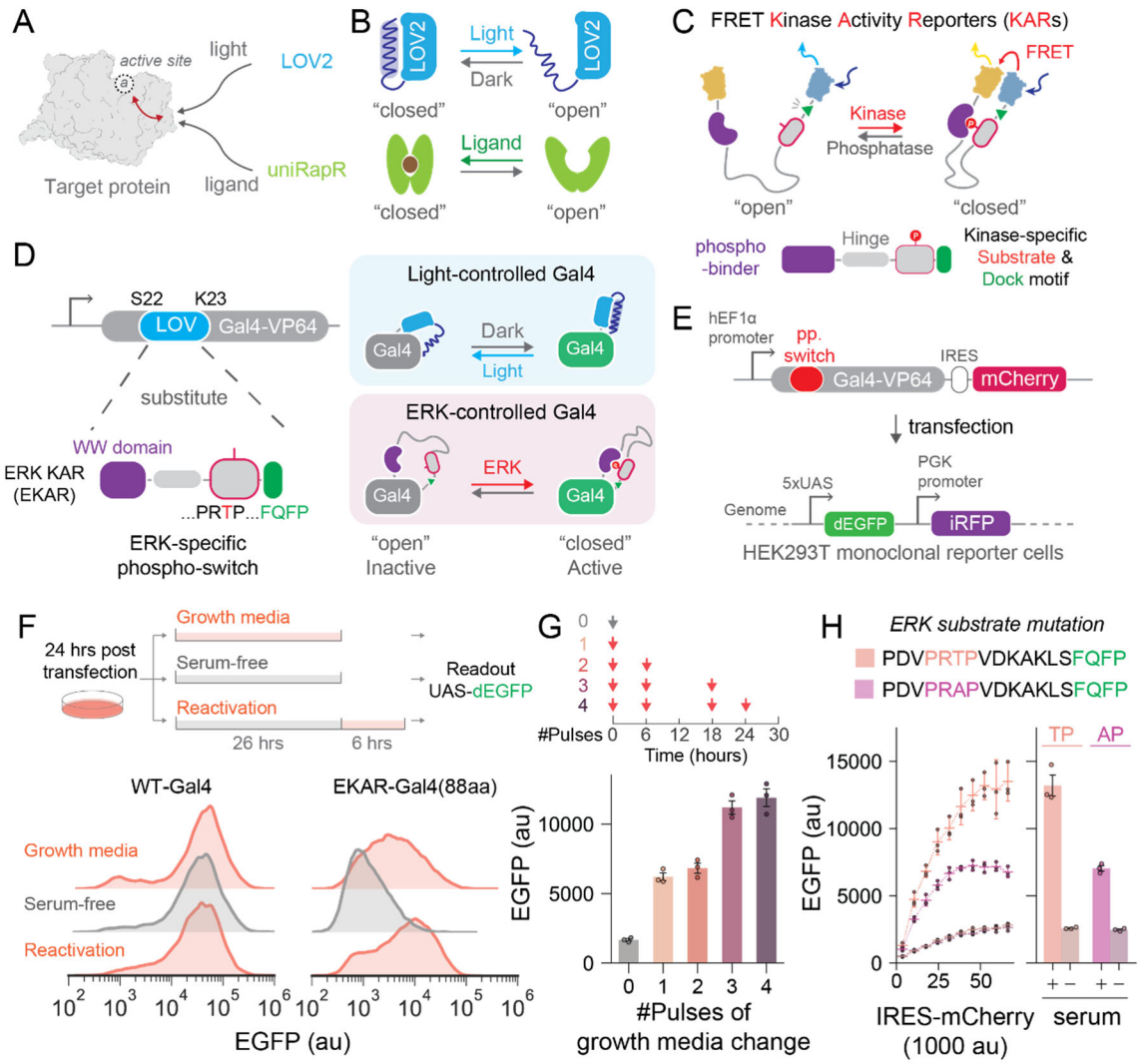

Figure 1. Repurposing FRET kinase activity biosensors as allosteric switches. (**A**) Schematic of engineered allosteric control of protein function. A stimulus-regulated protein domain, like light-sensitive AsLOV2 (blue) or ligand-sensitive uniRapR (green), is inserted into an allosteric site in a target protein and coupled to its function. (**B**) Mechanism of action for existing light/ligand-sensitive switches, which undergo a stimulus-dependent conformational change. (**C**) Schematic of FRET-based Kinase Activity Reporters (KARs). Fluorescent proteins on the N and C termini are linked by a phospho-binding domain (purple), a hinge region (gray) and a kinase-specific substrate (red) with docking motif (green). (**D**) The Gal4 DNA binding domain was previously made light-switchable by AsLOV2 insertion between Ser22 and Lys23. Replacing AsLOV2 with the ERK KAR (EKAR) produces a candidate ERK-controlled phosphoGal4 (EKAR-Gal4). (**E**) Overview of EKAR-Gal4 testing pipeline. EKAR-Gal4 was transiently expressed with an expression marker (IRES-mCherry) in a monoclonal 5xUAS-dEGFP HEK293T reporter cell line and EGFP expression was monitored in ERK-ON and ERK-OFF conditions. (**F**) Serum-dependent GFP expression of reporter cells transfected with Gal4-VP64 (WT-Gal4) or EKAR-Gal4. Cells were incubated in serum-free or growth media for 26 h before measurement. Reactivation was measured 6 h after switching back to growth media. Histogram represents >10000 cells combined from 3 replicates. (**G**) GFP expression in response to repeated growth media stimulation in EKAR-Gal4 expressing reporter cells. Error bars represent mean ± s.e.m (n = 3 replicates). (**H**) GFP expression in reporter cells expressing EKAR-Gal4 (PRTP) or its non-phosphorylatable T-to-A mutant (PRAP) in serum-free or growth media conditions. Curves present GFP expression across a range of TF expression levels (4 curves shown, with the serum-free conditions overlapping for PRTP and PRAP variants). Error bars on the curve represent the mean ± 95% confidence interval. Error bars in the right bar graph represent mean ± s.e.m (n = 3 replicates).

the resulting fusion protein EKAR-Gal4. When ERK is active, the WW domain would be expected to bind the phosphorylated peptide, resulting in a closed switch and a transcriptionally active Gal4 (**Fig. 1D**).

To assess the kinase-controlled activity of EKAR-Gal4, we used a previously developed clonal HEK293T cell line in which EGFP expression is driven by a Gal4-responsive *5xUAS* promoter (*5xUAS*-dEGFP) (**Fig. 1E**)[21]. We transiently transfected these cells with an EKAR-Gal4 plasmid that also included IRES-mCherry marker to assess cells' relative Gal4 expression levels (**Fig. 1E**). We then incubated cells in either serum-free media to induce an ERK-OFF state or serum-containing growth media to maintain the ERK-ON state (see **Methods**; for flow cytometry analysis pipeline see **Fig. S1**). We observed approximately three-fold higher EGFP expression from cells incubated for 26 h in growth media compared to serum-free media (**Fig. 1F**). We also found that EKAR-Gal4-induced EGFP expression could be reactivated within 6 h after a switch back from serum-free to growth media (**Fig. 1F**). In contrast, cells expressing an unmodified Gal4-VP64 transcription factor ("WT-Gal4") exhibited high levels of EGFP induction in both serum-free and growth media conditions (**Fig. 1F**).

ERK signaling can be dynamic, with cells only transiently entering an ERK-high state after growth factor stimulation[22–24], which might limit the extent of Gal4 transcriptional activity in our system. To test if this was the case in HEK293Ts, we characterized ERK dynamics after growth media stimulation using an ERK biosensor (ErkKTR) that is exported from the nucleus in response to ERK activation[25]. We found that ERK is only transiently activated for ~1 h by growth media stimulation in HEK293 cells and that after adaptation, cells can be activated again by exchanging the media for fresh growth media (**Fig. S2**). Based on these results, we hypothesized that a series of growth media exchanges might produce a higher Gal4 response. Indeed, the level of EKAR-Gal4-induced EGFP expression was correlated to the number of growth media exchanges delivered within 30 hours (**Fig. 1G**). For all subsequent experiments, we exchanged media at 0, 6, 18, 24 h prior to quantification of EKAR-Gal4 transcriptional output at 30 h.

We next sought to confirm that the change in EKAR-Gal4 transcriptional activity depends on the phospho-peptide's phosphorylation state. We made an EKAR-Gal4 variant with a threonine-to-alanine mutation in the consensus ERK phosphorylation site (PRTP to PRAP). In ERK-ON conditions, the PRAP mutant exhibited reduced transcriptional activity compared to the PRTP variant, but higher activity than cells in serum-free media (**Fig. 1H**). This data suggests that EKAR-Gal4 transcriptional activity is controlled by serum factors beyond a single phosphorylation event, an undesirable effect for our system and a primary target for optimization in subsequent experiments.

In summary, our initial experiments suggest that EKAR insertion is a promising starting point for the development of an ERK-controlled phospho-switch. However, further optimization is essential to improve its low potency, limited dynamic range, and residual activity in the T-to-A mutant. For version control purposes, we term this original EKAR as "phospho-switch v0" and the corresponding EKAR-Gal4 as "ERK-phosphoGal4v0".

163 **Hinge optimization reveals allosteric switch design principles**

164 As a first target for phospho-switch optimization, we examined the hinge region that links the
165 phosphorylatable peptide to the WW phospho-binding domain. Prior studies of FRET kinase
166 biosensors revealed that varying the length of this hinge can have substantial effects on biosensor
167 efficacy, with longer hinges typically producing a lower baseline of FRET activity and higher
168 biosensor gain[18]. However, the optimal hinge for an allosteric switch may differ substantially from
169 that of a FRET biosensor. We thus set out to explore a broad design space of hinge sequences,
170 focusing on improving the maximum activation in ERK-ON conditions and dynamic range
171 between ERK-ON and ERK-OFF conditions as design goals.

172 We constructed a combinatorial Golden-Gate cloning system (QCTK) for rapidly generating
173 allosteric switch variants (**Fig. 2A**; see **Methods**). We designed level 1 "a", "b", and "c" parts
174 consisting of phospho-binding domains, hinge sequences, and phosphorylatable substrates,
175 respectively (**Table S1-2**). These parts can be assembled with level 0 parts to construct the
176 expression plasmids of target protein with desired switch variant insertions, through a one-pot
177 reaction to clone individually or in a pooled manner. We first built a hinge library containing 26
178 hinge designs (1b_001-1b_026) in the context of EKAR's WW domain phospho-binder (1a_001)
179 and ERK-phosphorylatable substrate (1c_001). We focused on synthetic hinges of different lengths
180 in three major classes: long, flexible GS-rich peptides, alpha helical EAAAK-repeat sequences,
181 and proline-rich AP-repeat sequences. Some natural hinges with known secondary structures were
182 also included (**Fig. 2B**).

183 All switch variants were assembled into the Gal4 backbone (Part 0_001) and transiently
184 transfected into HEK293T *5xUAS*-dEGFP cells. Transfected cells were either starved or stimulated
185 with 4 growth media exchanges (**Fig. 1G**) and analyzed by flow cytometry to estimate the
186 phosphorylation-dependent change in transcriptional activity. We identified many hinge variants
187 with stronger maximum activation compared to our initial EKAR sequence (**Fig. 2C**; v0). Plotting
188 the fold-change and maximum activation for all 26 hinges revealed individual variants with high
189 scores on both metrics (**Fig. 2D**), and we chose 1b_001 (7aa EAAAKEA hinge) as the starting
190 point for future phospho-switch engineering (**Fig. 2D**; arrow), terming this variant "phospho-
191 switch v1".

192 Further examination of the hinge library responses revealed some design principles. First, it
193 enabled comparison of variants from different classes but with the same length. We found that
194 maximum activity in ERK-ON condition followed the pattern: GS-rich flexible > EAAAK helices >
195 AP proline-rich sequences, consistent with the interpretation that increasing rigidity in the hinge
196 interferes with forming the switch-closed state and reduces maximum Gal4 activity (**Fig. 2E**).
197 However, GS-rich flexible hinge variants tended to exhibit strong background activity, resulting
198 in a low fold change between ERK-OFF and ERK-ON conditions (**Fig. 2E;** hinge classes are color
199 coded as in **Fig. 2D**). In contrast, EAAAK/AP hinges showed a high fold change even at a short
200 length, suggesting that higher hinge rigidity is better able to maintain a switch-open state in the
201 absence of phosphorylation (**Fig. 2E**).

202 Second, the hinge library allowed us to assess performance of variants from the same class but
203 with different lengths. We observed that increasing GS linker length correlated with lower
204 background activity, as has been observed for FRET biosensors[18]. However, unlike FRET, we
205 found that longer hinges also reduced the maximum EGFP output, leading to a lower overall fold
206 change (**Fig. 2F**). These design principles are consistent with our top hit being a short but relatively

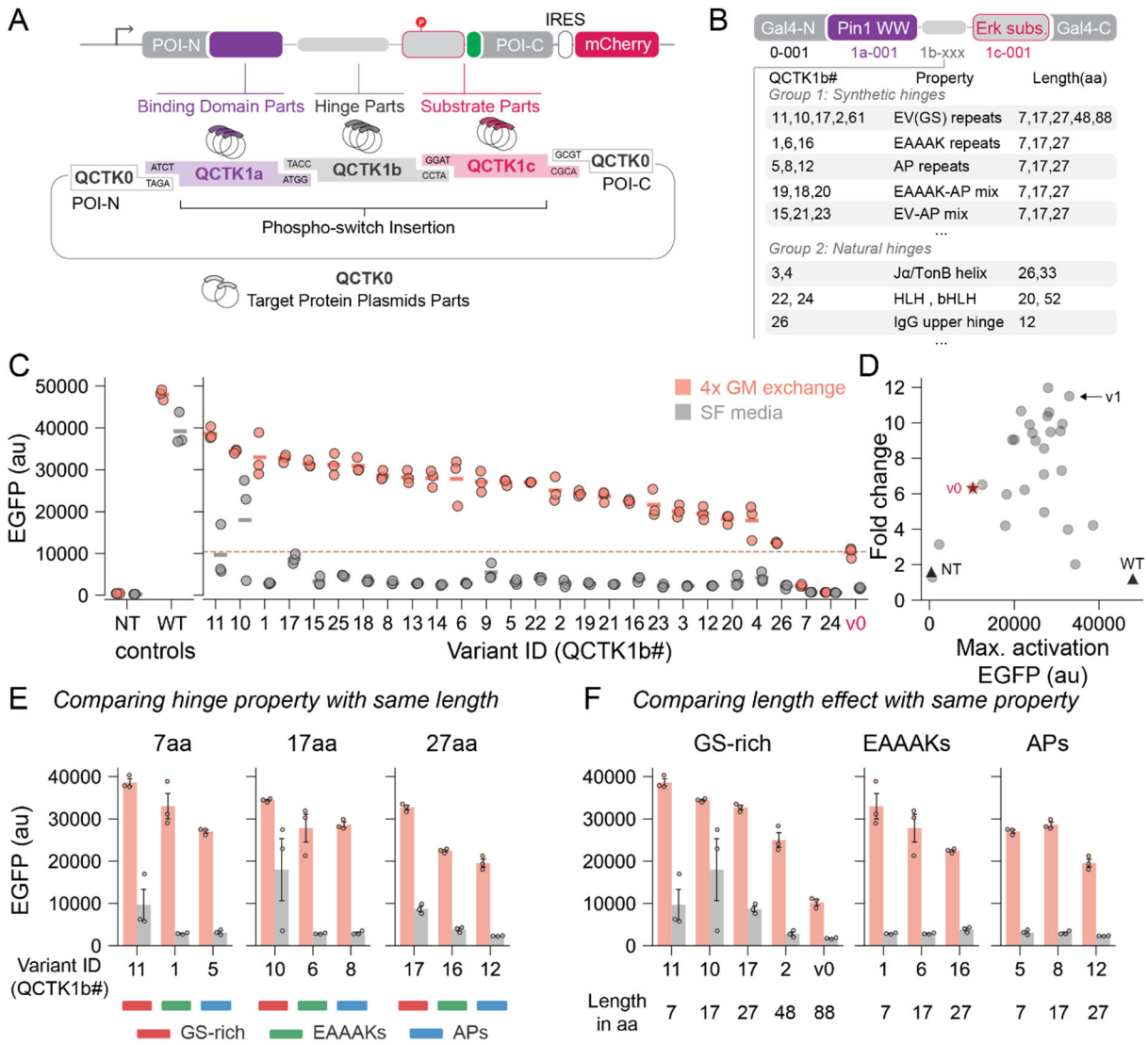

Figure 2. Combinatorial cloning to systematically optimize the hinge in the ERK phospho-switch. (**A**) Schematic of combinatorial Golden-Gate cloning system (QCTK) for rapid phospho-switch variants generation. Three components of the phospho-switch – the phospho-binding domain, hinge, and substrate – are designated as Level 1a, 1b, and 1c parts, respectively. The backbone including the promoter, Gal4 sequences and mCherry marker is designated as Level 0 parts. Assembled plasmids can be immediately transfected and tested in cells. (**B**) Overview of the hinge library. PhosphoGal4 variants were generated for all 26 hinge designs (1b_001-1b_026) with fixed parts for a Pin1 WW domain phospho-binder (1a_001), EKAR biosensor ERK substrate (1c_001) and backbone (0_001). (**C**) Transcriptional responses of all hinge variants in ERK-ON and ERK-OFF conditions. Cells transiently expressing each variant were either kept in serum-free (SF) media or stimulated with four growth media (GM) changes in 30 h before flow cytometry measurements. Bars indicate mean, and 3 replicates are shown as scattered dots. The red dashed line and axis label indicate the performance of the v0 (EKAR) initial design. NT, no transfection; WT, unmodified Gal4-VP64. (**D**) 2D plot of the fold-change and maximum activation for all 26 hinge variants. Red star: v0 (EKAR). Black triangles: no-transfection control (left) and WT-Gal4 control (right). Arrow indicates 1b_001 as an optimal hinge with high fold-change and maximum activation. Hinges are color-coded as: GS-rich (red); EAAAK-repeat helices (green); AP-repeat proline-rich (blue); other sequences (gray). (**E**) Comparison of hinge variants of the same length from different classes. 3 synthetic hinge classes are color-coded as in **D**. Error bars represent mean ± s.e.m (n = 3 replicates). (**F**) Comparison of variants of different lengths from the same class. Error bars represent mean ± s.e.m (n = 3 replicates).

208 rigid variant: a 7 amino acid helical hinge. We fitted a multi-variable regression model with
209 experimental hinge data to predict corresponding switch performance (see **Methods**; **Fig. S3A-C**).
210 In predicting the response of additional computer-generated sequences, the model recapitulated
211 the observed patterns for hinge rigidity and length, suggesting that rigid EAAAK- and AP-repeat
212 sequences exhibited an optimal balance of maximum activation and sensitivity to phosphorylation
213 (**Fig. S3D-F**).

214 We used AlphaFold3[26] to predict the structures of both phosphorylated and unphosphorylated
215 ERK phospho-switch v1 in Gal4 (**Fig. S4**), which captured the binding event between the WW
216 domain and phosphorylated ERK substrate, matching previous structural studies of the WW-
217 peptide interaction[27]. We also measured ERK-phosphoGal4v1 performance after inserting
218 additional linker residues between the phospho-switch and Gal4 DNA binding domain, which
219 should weaken allosteric coupling between these domains (**Fig. S5A**). Indeed, we observed
220 decreasing ERK-switchable behavior with increasing linker length, consistent with allosteric
221 coupling that is weakened by longer, more flexible linkers (**Fig. S5B**).

222

223 **Improving the substrate site and phospho-binder to generate an optimal phospho-switch**

224 Although our initial phospho-switches exhibited good switching between serum-free and
225 growth media conditions, we found that a non-phosphorylatable mutant switch still retained
226 modest residual EGFP expression in growth media (**Fig. 1H**). We set out to understand and reduce
227 this effect, initially hypothesizing that the residual activity might be due to phosphorylation at
228 additional sites in the substrate peptide that leads to WW domain binding and Gal4 activation.

229 We constructed a series of phospho-switches harboring mutant substrate peptides (variants of
230 part 1c in the Golden Gate toolkit; **Fig. 3A**) that were designed to eliminate potential ERK-
231 phosphorylatable Ser/Thr residues (Substrates 2-4). We also included a peptide that eliminates all
232 phosphorylatable residues, phospho-mimetic residues, and proline residues, any of which could
233 contribute to WW domain binding (Substrate 5). We found that the presence of the
234 phosphorylatable PRTP motif ensured strong serum-dependent EGFP expression regardless of
235 these additional sequence modifications (**Fig. 3B**), and only Substrate 5 completely abolished
236 residual EGFP expression in growth media (**Fig. 3B**). Based on these data, we designed a final pair
237 of peptides in which the phosphorylatable PRTP or non-phosphorylatable PRAP motif was re-
238 introduced into the otherwise-noninteracting Substrate 5 peptide (**Fig. 3C**). A single Pro-directed
239 phosphorylation site was able to rescue high transcriptional output in growth media, and the
240 corresponding non-phosphorylatable PRAP variant exhibited a 42% reduction in background
241 activity compared to the original ERK-phosphoGal4v1 design (**Fig. 3C**). This new variant, termed
242 "phospho-switch v2", exhibits a similar maximum activation level, but because of the decrease in
243 background, shows a 1.7-fold increase in dynamic range between PRTP and PRAP variants in
244 growth media compared to the v1 design (**Fig. 3G**).

245 We hypothesized that residual activity could be further reduced by targeted mutations in the
246 WW domain to decrease its affinity for the unphosphorylated substrate. Structural and biochemical
247 studies have determined that specific residues in the WW domain, Arg14 and Phe25, make contacts
248 to the first proline residue in the PRTP site and contribute to binding in a phosphorylation-
249 independent manner (**Fig. 3D**)[28,29]. We constructed phosphorylatable and non-phosphorylatable
250 versions of the ERK-phosphoGal4v2 scaffold in which these two residues were mutated to Ala and

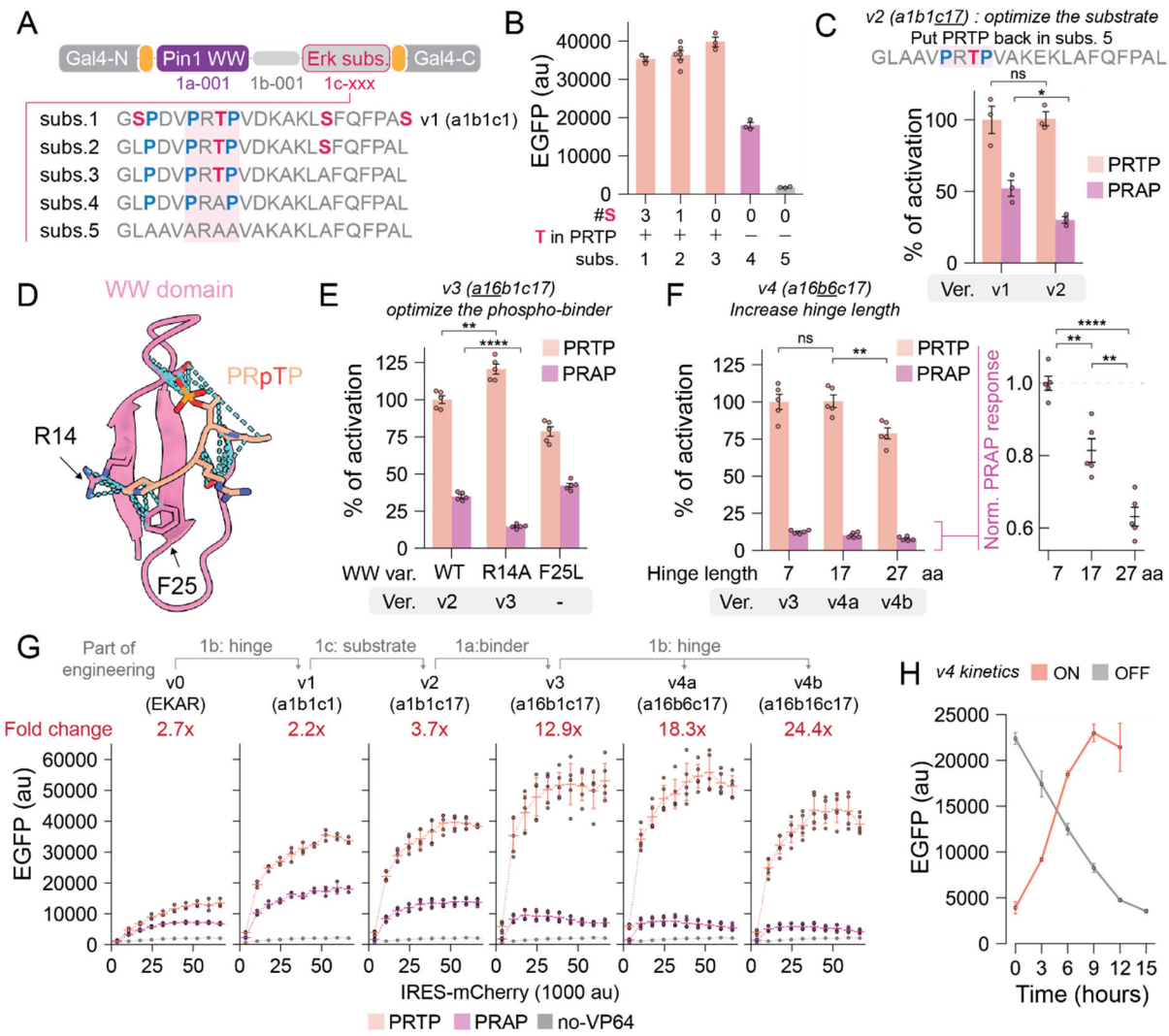

Figure 3. Substrate and phospho-binder optimization for an optimal ERK phospho-switch. (**A**) Overview of mutant substrate peptides. ERK-phosphoGal4v1 (substrate 1) was modified to include substrate peptide variants (substrates 2-5) by mutating phosphorylatable, proline, and negatively charged residues that might contribute to WW domain binding. (**B**) GFP expression of phosphoGal4 variants. Cells transiently expressing variants were stimulated with four growth media changes in 30 h before flow cytometry measurements. Error bars represent mean ± s.e.m (n = 3-6 replicates). (**C**) Reintroducing the ERK-consensus phosphorylation motif (PRTP or non-phosphorylatable PRAP as control) into the noninteracting peptide (subs. 5) increases the switch's dynamic range. The best-performing variant (a1b1c17) is termed the "v2" phospho-switch. Error bars represent mean ± s.e.m (n = 3 replicates). (**D**) AlphaFold3-predicted model of the Pin1 WW domain (pink) interacting with PRpTP (phosphorylated PRTP peptide, orange). Arrows indicate positions of Arg14 and Phe25. Blue dash lines indicate predicted contacts. (**E**) Characterization of ERK-phosphoGal4v2 variants with WW domain mutations in phosphorylatable (PRTP) and non-phosphorylatable (PRAP) contexts. The resulted optimal variant (a16b1c17) terms as "v3". Error bars represent mean ± s.e.m (n = 5 replicates). (**F**) Characterization of ERK-phosphoGal4v3 variants with increasing length of helical hinges in phosphorylatable (PRTP) and non-phosphorylatable (PRAP) contexts. The 2 result variants (a16b6c17 and a16b16c17) are termed "v4a" and "v4b". Error bars represent mean ± s.e.m (n = 5 replicates). (**G**) Overall course of optimization from v0 (EKAR) to v4a/b (a16b6/16c17). Performance of each version is presented as GFP expression curves across a range of TF expression levels. Error bars on the curve represent the mean ± 95% confidence interval (n = 3-5 replicates). Phosphorylatable (PRTP), non-phosphorylatable (PRAP), and a no-VP64 phosphoGal4v3 variant were tested. (**H**) ON/OFF kinetics of ERK-phosphoGal4v4a in stably expressing cells. 24 h after seeding, cells were incubated in serum-free media for OFF kinetics. 18 h post starvation, cells were switched into growth media culture for ON kinetics. Error bars on the curve represent the mean ± s.e.m (n = 3 replicates). For all panels, statistical significance was computed using the two-tailed Student's t-test. p-value annotation: ns, $p > 0.05$; *, $0.01 < p <= 0.05$; **, $10^{-3} < p <= 0.01$; ***, $10^{-4} < p <= 10^{-3}$; ****, $p <= 10^{-4}$.

251

252 Leu, respectively[28,29]. We found that while the F25L mutation had an undesirable effect by
253 reducing maximum activation, the R14A variant still drove strong EGFP expression in growth
254 media conditions and exhibited a further 58% reduction in basal activity from a non-
255 phosphorylatable variant compared to ERK-phosphoGal4v2 (**Fig. 3E**). We termed this variant
256 "phospho-switch v3". As a final improvement, we revised our hinge design to further weaken
257 substrate-WW interactions by increasing the length of the helical hinge from 7 aa to 17 aa or 27
258 aa, producing "phospho-switch v4a" or "v4b" with further reduction in background activity (**Fig.
259 3F**).

260 Over the course of optimization from our phospho-switch v0 to v4a/b designs, the dynamic
261 range of the engineered TF increased from 2.7-fold to 24.4-fold between phosphorylated and
262 unphosphorylated conditions and the maximum activation increased 3.5- to 4.6-fold (**Fig. 3G**; **Fig.
263 S6**). Our EKAR-phosphoGal4v4a reaches a comparable level of gene expression to unmodified
264 Gal4, and the non-phosphorylatable mutant is comparable to a negative control Gal4 construct that
265 lacks the VP64 transactivation domain (**Fig. S6**). We measured the kinetics of EGFP accumulation
266 and loss in response to media changes in *5xUAS*-dEGFP HEK293T cells that stably express the
267 ERK-phosphoGal4v4a construct, observing activation and inactivation with a half-life of ~6 h (**Fig.
268 3H**). Finally, we tested the ERK-phosphoGal4v4a system across multiple cellular contexts,
269 including in mouse embryonic stem cells and fibroblasts, where we observed EGFP expression in
270 response to serum stimulation that was eliminated by treatment with a MEK inhibitor (**Fig. S7**).
271 We thus conclude that our ERK phospho-switch v4 is an optimized phosphorylation-actuated
272 protein switch that can be used to achieve potent and reversible control over gene expression in
273 the context of an allosterically-controlled Gal4-VP64 transcription factor.

274

275 **Direct and specific activation of ERK-phosphoGal4 using optogenetics**

276 Media switch experiments are a simple method to alter ERK activity for characterizing
277 candidate ERK-phosphoGal4 designs. However, growth media contains complex mixtures of
278 growth factors and other molecules that can alter the activity of many intracellular pathways. We
279 thus set out to characterize our ERK-phosphoGal4 system in response to stimuli that specifically
280 and uniquely activate the ERK cascade. We reasoned that such an approach might also aid in better
281 understanding the residual EGFP expression observed from our v0-v2 non-phosphorylatable
282 switch variants in growth media conditions (**Fig. 1H; Fig. 3G**).

283 We turned to our previously-developed OptoSOS optogenetic system as a method to directly
284 activate the Ras/ERK pathway[30,31]. We engineered *5xUAS*-dEGFP HEK293T cells that stably
285 expressed a blue-light-responsive variant of this OptoSOS system[31,32], the ERK-phosphoGal4v2
286 transcription factor, and the ErkKTR-iRFP biosensor (**Fig. 4A-B**). Continuous blue light
287 stimulation drove sustained nuclear export of the ErkKTR biosensor, indicative of sustained ERK
288 activity, and also produced strong EGFP expression in serum-free media (**Fig. 4C**; **Fig. S8**). The
289 light-induced response could be eliminated by treatment with 10 μM of the MEK inhibitor PD
290 0325901 (**Fig. 4D**). Light-induced EGFP expression could be tuned by varying the intensity or
291 duty cycle of illumination, with increasing EGFP output as the duration of light pulses increased
292 from 2.5' every 30' to continuous illumination at 2 mW/cm^2 (**Fig. 4E-F**). These data indicate that
293 ERK-phosphoGal4 activity can be tuned to intermediate levels by minute-timescale changes in
294 ERK activity, suggesting that the transcription factor is able to rapidly switch between active and
295 inactive states upon phosphorylation in response to these fast changes in illumination conditions.

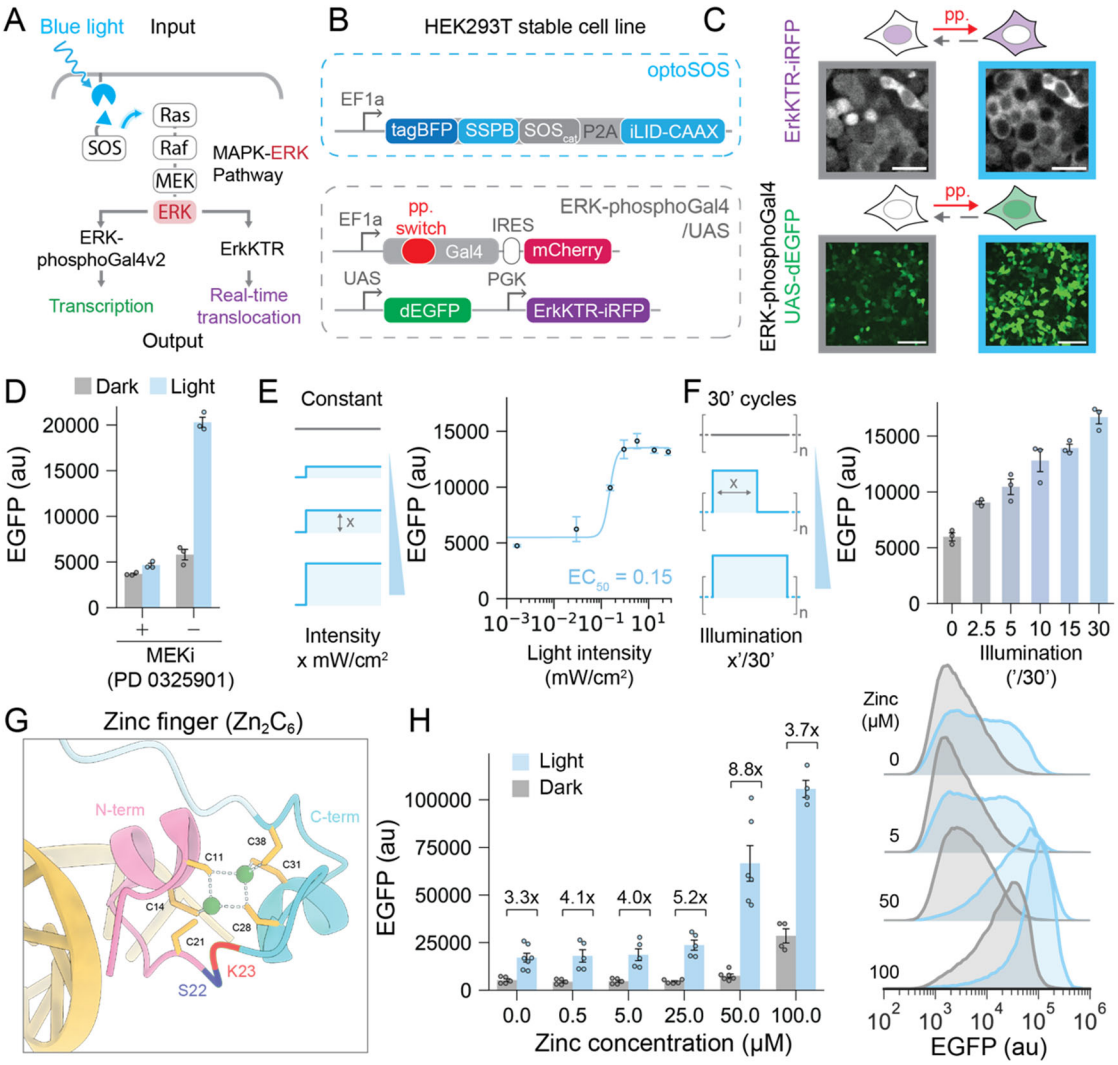

Figure 4. Direct and specific activation of ERK-phosphoGal4 with optogenetics. (**A**) Schematic of optogenetic ERK stimulation and measurements. Blue light induced membrane association of SOS activates the Ras-ERK cascade. ERK activity is directed to the real-time nuclear-to-cytosolic translocation of the ErkKTR biosensor as well as EGFP production through the ERK-phosphoGal4v2/UAS system. (**B**) Overview of the optogenetic HEK293T stable cell line. Cells constitutively express optoSOS, ErkKTR-iRFP, ERK-phosphoGal4v2 and harbor a *5xUAS*-dEGFP reporter. (**C**) Representative images of ErkKTR translocation and ERK-phosphoGal4 induced GFP expression in light and dark. Top panel shows ErkKTR localization before and after 1 h blue light illumination (Scale bar, 25 μm). Bottom panel shows GFP expression before and after 10 h blue light illumination (Scale bar, 100 μm). (**D**) MEK inhibition of ERK-phosphoGal4v2/UAS response to optogenetic ERK stimulation. Cells were incubated in dark or continuous light illumination at 2 mW/cm^2 for 22 h with or without the presence of 10 μM PD 0325901 and analyzed by flow cytometry. Error bars represent mean ± s.e.m (n = 3 replicates). (**E**) Light-induced GFP expression in response to light intensity levels. Cells were continuously illuminated at various intensities for 22 h and analyzed by flow cytometry. Error bars on the curve represent the mean ± 95% confidence interval (n = 3 replicates). The data is fitted to a Hill curve for estimation of the EC50. (**F**) Light-induced GFP expression in response to illumination duty cycles. Cells were illuminated with various duty cycles ranging from 2.5' every 30' to continuous illumination at 2 mW/cm^2 for 22 h and analyzed by flow cytometry. Error bars represent mean ± s.e.m (n = 3 replicates). (**G**) Crystal structure of Gal4 Zn_2C_6 zinc finger (PDB: 3COQ). 6 cysteines (C11, C14, C21, C28, C31, C38) coordinate with 2 zinc ions (green). Conformational switching of a stimulus-sensitive domain between Ser22 (dark blue) and Lys23 (red) is expected to separate the zinc finger into N-terminal (pink) and C-terminal (light blue) halves that may interfere with zinc coordination. (**H**) GFP expression in dark/light conditions in response to media zinc concentration. Cells were incubated in serum-free media supplemented with various levels of $ZnCl_2$ in dark or continuous illumination at 2 mW/cm^2 for 22 h and analyzed by flow cytometry. Error bars represent mean ± s.e.m (n = 4-7 replicates). Histograms show >25000 cells across all replicates.

297 We also used the simplicity of optogenetic stimulation to further investigate how serum might
298 affect Gal4 activity independently of ERK. The SK22 insertion site is located inside the Zn_2C_6
299 zinc finger (ZF) domain nearby cysteine residues that are essential for Zn^{2+} coordination (**Fig.**
300 **4G**)[33]. We hypothesized that the allosteric switch might switch the Gal4 DNA binding domain
301 between zinc-bound and zinc-unbound states. In this model, high zinc ion concentrations could
302 shift the equilibrium to favor the zinc-bound, active Gal4 conformation even in the absence of
303 ERK phosphorylation. Such a model could help explain the difference in activity observed for a
304 non-phosphorylatable variant in serum-free and growth media conditions, as the 1-40 μM levels
305 of Zn^{2+} in tissue culture media is primarily provided by serum[34,35]. To test this model, we used the
306 OptoSOS system to activate ERK in serum-free media supplemented with varying concentrations
307 of $ZnCl_2$. Indeed, we observed that high zinc concentrations increased EGFP induction in both
308 illuminated (ERK-ON) and unilluminated (ERK-OFF) conditions (**Fig. 4H**). These data are
309 consistent with a model where high zinc concentrations act in concert with residual WW-peptide
310 binding to shift the equilibrium of ERK-phosphoGal4v2 to the transcriptionally-active
311 conformation. We note that our improved v4 phospho-switches already eliminate serum-induced
312 activity from the non-phosphorylatable PRAP variant, likely by reducing the WW-peptide binding
313 affinity to shift the equilibrium to the switch-open, zinc-unbound state even under growth media
314 conditions.

315

316 **ERK-phosphoGal4 outperforms the FOS promoter for sensing ERK activity**

317 Transcriptional biosensors are widely used for assessing signaling pathway activity in high-
318 throughput screens and for reporting on spatiotemporal signaling in multicellular contexts[36–38].
319 Most transcriptional biosensors are constructed from signaling-responsive endogenous enhancers
320 and promoters[39–41]. These classic reporters suffer from two drawbacks. First, they can lack
321 specificity: endogenous enhancers contain binding sites for many transcription factors and thus
322 their expression is not exclusively determined by the activity of a single kinase. A second challenge
323 is availability, as many endogenous kinases do not drive specific transcriptional responses and thus
324 lack well-defined transcriptional biosensors. We reasoned that one immediate use of our
325 engineered phosphorylation-switchable TF could be as a direct transcriptional biosensor of kinase
326 activity that is more specific for ERK signaling than traditional systems based on endogenous
327 promoters.

328 We set out to compare our optimized ERK-responsive transcription factor (ERK-
329 phosphoGal4v4a) to a 2.5 kb *c-fos* upstream regulatory sequence (P_{FOS}). While P_{FOS} has been
330 widely used to report on ERK activity[42–44], it contains multiple TF binding sites including cAMP
331 responsive elements (CRE), serum responsive elements (SRE) and AP-1 binding sites, which can
332 serve as targets for a wide range of additional pathways (e.g., PKA, calcium, PKC, and other
333 MAPKs) (**Fig. 5A**)[40,45]. Notably, P_{FOS} is also widely used as a calcium-responsive promoter of
334 neuronal activity[46,47]. We constructed stable HEK293T cell lines containing either *5xUAS*-dEGFP
335 or P_{FOS}-dEGFP that each includes a constitutively expressed iRFP marker using PiggyBac-
336 mediated genome integration[48]. Both lines were sorted with similar expressions of iRFP to ensure
337 similar strengths of each reporter. We also stably introduced ERK-phosphoGal4v4 into the *5xUAS*-
338 dEGFP cell line (**Fig. 5A**).

339 To assess each cell line's response to ERK-activating stimuli, we treated them with various
340 concentrations of serum after overnight incubation in serum-free media and analyzed EGFP

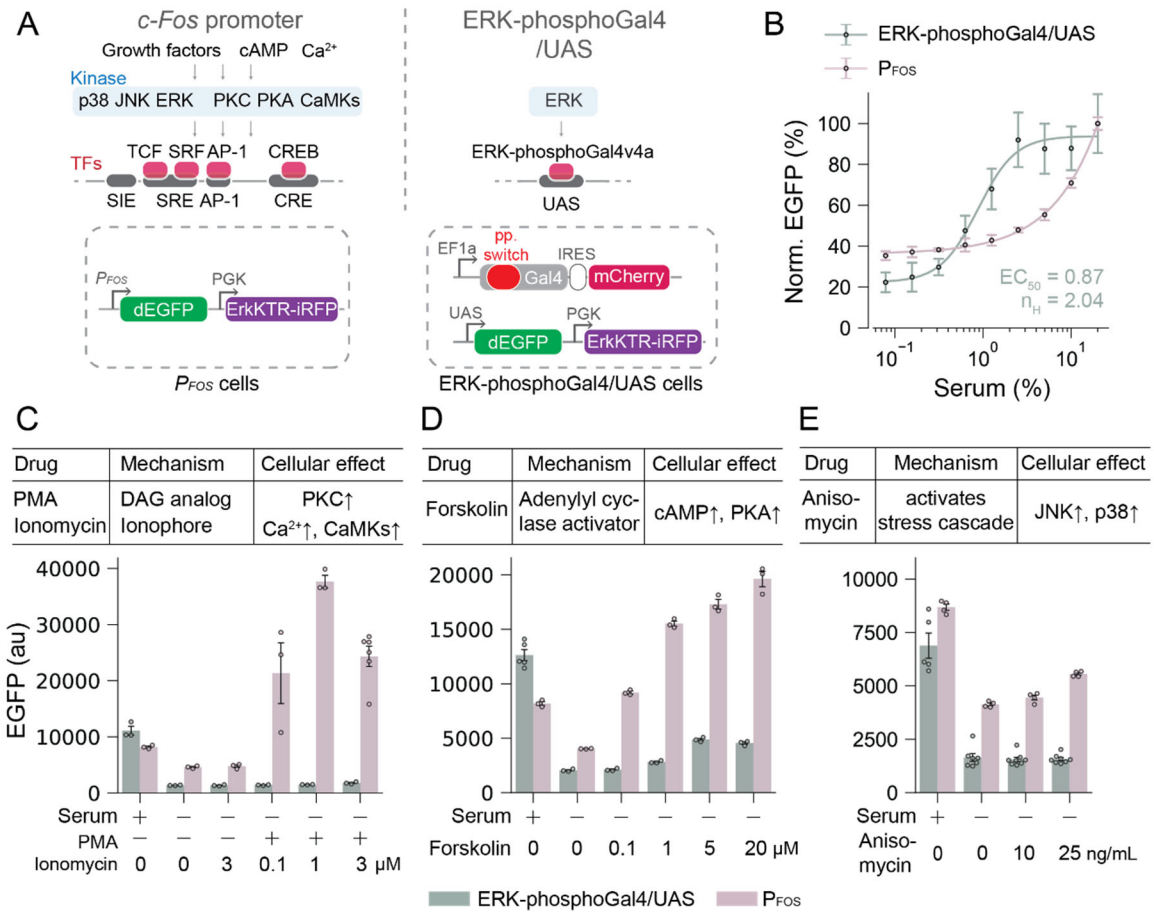

Figure 5. Comparison of ERK-phosphoGal4/UAS and *P*$_{FOS}$ promoter. (**A**) Schematic of ERK-to-transcription signal transmission for the *P*$_{FOS}$ promoter and the ERK-phosphoGal4v4a/UAS system. Two HEK293T cell lines were constructed to compare both reporting systems at similar strength, using ErkKTR-iRFP as an integration marker. (**B**) Serum dose-response curve for the *P*$_{FOS}$ promoter and the ERK-phosphoGal4v4a/UAS system. Cells were incubated in serum-free (SF) media overnight and treated with 0.1-20% serum for 4 h. Each curve is normalized to the maximum GFP expression. Error bars on the curve represent the mean ± 95% confidence interval (n = 3-5 replicates). The ERK-phosphoGal4v4a data is fitted to a Hill curve for estimation of the EC50 and Hill coefficient. (**C-E**): Comparison of *P*$_{FOS}$ and ERK-phosphoGal4v4a/UAS systems in cells stimulated with diverse signaling inputs including the PKC/calcium activators PMA and ionomycin (in **C**), the PKA activator forskolin (in **D**), and the JNK/p38 activator anisomycin (in **E**). Cells were pre-starved overnight and incubated in drug conditions for 4 h before flow cytometry measurements. Error bars represent mean ± s.e.m (n = 3-8 replicates). Serum conditions indicate standard growth media (10% FBS). In **C**, 30 nM PMA was used; all other drug conditions are as indicated on the figure.

expression by flow cytometry 4 h post-treatment. These experiments revealed striking differences between ERK-phosphoGal4v4a and the *P*$_{FOS}$ promoter (**Fig. 5B**). ERK-phosphoGal4v4 was activated with an EC50 of ~1% serum, consistent with measurements of serum-induced ERK activity[24]. Gene expression was induced by serum with a Hill coefficient of 2.0 that suggests modest cooperativity. In contrast, the *P*$_{FOS}$ response does not plateau even at relatively high serum concentrations of 20%. We also found *P*$_{FOS}$ to have high background activity in HEK293 cells when starved, resulting in a low dynamic range compared to ERK-phosphoGal4v4a (**Fig. 5B**). Finally, we compared both systems in the presence of other signaling activators: PMA/ionomycin to activate PKC and calcium signaling, forskolin to activate PKA, and anisomycin to activate the p38 and JNK MAPKs (**Fig. 5C-E**; **Fig. S9**). *P*$_{FOS}$ was even more strongly activated by PMA/ionomycin and forskolin than by serum stimulation and was also partially activated by

352 anisomycin treatment. In contrast, ERK-phosphoGal4v4a was insensitive to PMA/ionomycin and
353 anisomycin, with a mild response to forskolin treatment much lower than that observed in response
354 to serum stimulation. Taken together, these results suggest that our engineered ERK-responsive
355 transcription factor, ERK-phosphoGal4v4a, exhibits a well-defined dose response to ERK-
356 activating stimuli and low crosstalk to other intracellular signals, with superior performance
357 relative to P_{FOS}-based reporters.

358

359 **Phospho-switch control is generalizable to other input kinases and effector proteins**

360 Kinase-controlled allosteric switches have the potential to be powerful tools for synthetic
361 biology because of their generalizability to multiple inputs and outputs. At the input level, FRET
362 biosensors have been developed for many kinases, and these phospho-sites could also be
363 incorporated into our optimal switch backbone to rewire input specificity. At the output level, our
364 optimized phospho-switch could also be inserted into other allosterically controlled target proteins.
365 We thus set out to test whether our design could be extended to other input kinases and effector
366 proteins.

367 We first tested whether the phosphoGal4 design could be rewired to another input kinase (**Fig.**
368 **6A**). We turned to the JNK MAPK, a kinase which also has a well-characterized FRET biosensor
369 (JNKAR) but for which transcriptional biosensor options are limited. We assembled a JNK-
370 phosphoGal4 system using the "v2" (wild-type WW phospho-binder) and "v3" (WW^{R14A})
371 architecture, but where the ERK-specific substrate was exchanged for the JNK-specific JNKAR
372 substrate sequence. Each phospho-switch design was inserted into Gal4 at the same SK22
373 allosteric site (**Fig. 6B**) and transfected into *5xUAS*-dEGFP cells. Indeed, we found that cells
374 expressing a phosphorylatable JNK-phosphoGal4 construct induced EGFP expression in response
375 to the JNK activator anisomycin, with the "v3" design outperforming "v2" (**Fig. 6C**) as we had
376 previously observed for ERK (**Fig. 3G**). EGFP expression varied with anisomycin dose (**Fig. 6D**)
377 over a concentration range previously seen to activate JNK[25]. Importantly, our ERK-
378 phosphoGal4v4a system was not sensitive to anisomycin (**Fig. 5E**), so the observed response is
379 specific to the inclusion of a JNK-targeted substrate. In sum, our phospho-switch design is suitable
380 to be used for multiple input kinases.

381 We also tested whether the phospho-switch might also extend to other allosterically
382 controllable target proteins (**Fig. 6E**). We turned to OptoNanobodies, nanobodies into which we
383 previously inserted AsLOV2 to confer light-controlled binding to various target proteins: mCherry,
384 EGFP, and endogenous F-actin[49]. We replaced AsLOV2 in the F-actin OptoNanobody with our
385 "v3" variant ERK phospho-switch to generate a candidate ERK-phosphoNanobody (**Fig. 6F**). We
386 inserted the phospho-switch between amino acid positions 63-66, as previously done for AsLOV2
387 insertion (**Fig. 6G**), fused the construct to TagRFP to monitor its localization, and introduced it
388 into HEK293T cells that also expressed the ErkKTR biosensor to monitor ERK activity[25]. We then
389 assessed localization of the nanobody in growth media stimulated cells for both a phosphorylatable
390 (PRTP) and non-phosphorylatable (PRAP) switch, in the presence or absence of the MEK inhibitor
391 U0126.

392 Serum stimulation of ERK-phosphoNanobody cells resulted in rapid TagRFP relocalization
393 from the cytosol to the cell periphery (**Fig.6H-I; Mov. S1**), consistent with nanobody binding to
394 cortical F-actin[49]. This effect was not observed in cells expressing a non-phosphorylatable

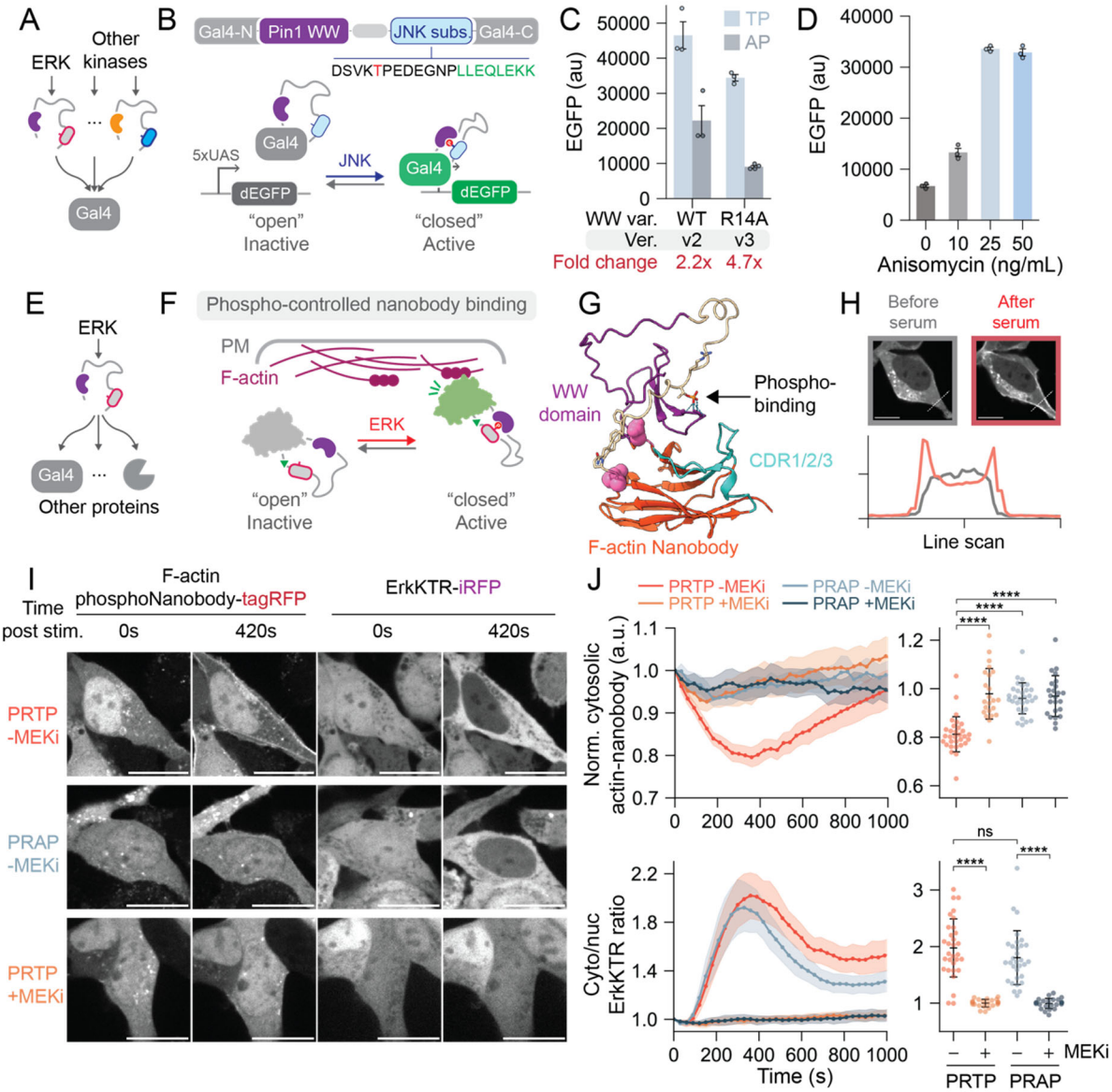

Figure 6. Phospho-switch control is generalizable to other input kinases and effector proteins. (**A**) Generalizing the phospho-switch to accept inputs from additional kinases. (**B**) A JNK-dependent phospho-switch was developed by including a JNK-specific substrate (phosphorylation site in red and docking motif in green). (**C**) Anisomycin-induced GFP expression of JNK-phosphoGal4v2 (harboring the wild-type Pin1 WW domain) and JNK-phosphoGal4v3 (harboring the WW^{R14A} domain) as compared to non-phosphorylatable T-to-A mutants. Cells transiently expressing each JNK-phosphoGal4 variant were incubated in serum-free (SF) media containing 25 ng/mL anisomycin for 24 h. (**D**) Anisomycin dose-response of JNK-phsphoGal4v3. Cells transiently expressing JNK-phosphoGal4v3 were incubated in SF media with various anisomycin concentrations for 24 h. For **C-D**, Error bars represent mean ± s.e.m (n = 3 replicates). (**E**) Generalizing the phospho-switch to control additional output proteins. (**F**) The ERK phospho-switch v3 was inserted into an anti-F-actin nanobody to generate an ERK-phosphoNanobody. (**G**) AlphaFold3-predicted model of the ERK-phosphoNanobody. The ERK phospho-switch was inserted between Asp63 and Gly66 (pink) of the F-actin nanobody (orange; CDR1/2/3 in cyan). Arrow indicates predicted contacts between the phosphorylated threonine and the WW domain (purple). (**H**) Serum-induced ERK-phosphoNanobody binding. Top panels: images of a representative cell before and after 7 min treatment with serum. Dashed lines indicate the position of a line scan for quantifying ERK-phosphoNanobody intensity. Scale bar, 10 µm. Bottom panels: quantification of ERK-phosphoNanobody fluorescence along the line scans before (gray) or after treatment (red) reveals translocation to the cell membrane upon serum stimulation as expected for cortical actin binding. (**I**) Representative ERK-phosphoNanobody and ErkKTR images before and after serum treatment in the presence or absence of 10 µM U0126, a MEK inhibitor. A non-phosphorylatable T-to-A variant was tested as a control. Scale bar, 20 µm. (**J**) Quantification of ERK-phosphoNanobody and ErkKTR response to serum stimulation. Left panels show time traces of cytosolic ERK-phosphoNanobody fluorescence intensity and cytosolic-to-nuclear ErkKTR ratio over time after serum stimulation

at 0 sec. Mean trajectories (solid lines) are shown with shading representing the 95% confidence interval. Right panels show single cell responses 7 min after serum treatment. Error bars represent mean ± s.d (For both panels: PRTP -MEKi, n = 31 cells; PRTP +MEKi, n = 23 cells; PRAP -MEKi, n = 31 cells; PRAP +MEKi, n = 24 cells. Cells are quantified from 2-3 independent experiments). Statistical significance is verified with Mann-Whitney-Wilcoxon tests (two-sided with Bonferroni correction). p-value annotation: ns, $p > 0.05$; *, $0.01 < p <= 0.05$; **, $10^{-3} < p <= 0.01$; ***, $10^{-4} < p <= 10^{-3}$; ****, $p <= 10^{-4}$.

nanobody variant and was also abrogated by treatment with 10 μM of the MEK inhibitor U0126, which blocked ERK activity as measured by redistribution of the ErkKTR biosensor (**Fig. 6I; Mov. S2-4**). We quantified the response by measuring the nanobody's cytosolic fluorescence intensity, which decreased upon redistribution of the nanobody to cortical F-actin after serum stimulation. Nanobody cytosolic clearance peaked at 6 min after serum stimulation before partially adapting back to baseline within 10-15 min (**Fig. 6J**, upper panel), closely matching the dynamics of ErkKTR translocation (**Fig. 6J**, lower panel). These data suggest that like the ErkKTR biosensor, the ERK-phosphoNanobody rapidly tracks changes in ERK kinase activity. We further tested whether differences in performance could be observed for ERK-phosphoNanobodies harboring "v2" or "v3" versions of the phospho-switch. Indeed, we observed more residual activity in the non-phosphorylatable "v2" phosphoNanobody compared to the "v3" variant with weakened WW binding affinity (**Fig. S10**), suggesting again that the optimized phospho-switch performs well across protein contexts. In sum, these data reveal that our kinase-controlled switch can indeed be generalized across multiple input kinases by swapping phospho-peptides from other FRET biosensors, and can be wired in to control multiple output proteins in which sites of stimulus-controlled allostery have been identified.

Discussion

Building customizable input/output interfaces with the cell's endogenous kinase networks is a grand challenge in synthetic biology, with diverse applications in cell engineering, biosensing, and the detection and reversion of disease-associated cellular states. However, our ability to engineer novel phosphorylation-regulated processes in the cell is still limited. Given a kinase and target protein of interest, how might the synthetic biologist draw a new link to trigger an output protein's activity in response to phosphorylation by an input kinase?

In the current study, we explore this broad question using a combination of recently developed tools. On the output side, engineered allosteric control has been successfully used to design stimulus-responsive variants of enzymes, kinases, transcription factors, and protein binders[15,16,21,49–52]. On the input side, FRET biosensors are available for an increasing number of kinases to convert a phosphorylation event to a conformational change in the biosensor[20]. We set out to link these two emerging approaches by engineering protein switches that convert phosphorylation by a specific kinase into an allosteric change in a target protein's activity. We find that these kinase-controlled allosteric switches serve as potent, reversible control points for protein function. Our optimized switch – the ERK phospho-switch v4 – can confer up to a 20-fold change in gene expression when inserted at a previously identified allosteric control point in the Gal4 DNA binding domain. The switch design also generalizes to multiple input kinases (ERK and JNK) and output proteins (Gal4 and an F-actin nanobody).

Our study also reveals key design features for the allosteric switch that differ from the original FRET biosensor. For example, we found that the flexible linkers that perform well for FRET make exceptionally poor allosteric switches regardless of length, and that short, rigid linkers combine high maximum activation with low leakiness. We also find that residual binding affinity between

435 the phospho-binding domain and unphosphorylated substrate can be deleterious and identify
436 mutations in both the phospho-binder and substrate that improve the phospho-switch's dynamic
437 range. Thus, while an ERK-responsive FRET biosensor serves as a useful starting point for switch
438 engineering, optimal phospho-switch performance required substantial additional engineering. It
439 is possible that these advances (e.g. WW domain mutations; short rigid hinge sequences) could be
440 ported back to FRET biosensors to further optimize their performance. Alternatively, some of these
441 design constraints may be unique to the phospho-switch, where a target protein is fused to the
442 switch's N and C termini and likely exerts forces on them that are not present in the FRET
443 biosensor framework.

444 Throughout this study we focus on one model system for allosteric control: an engineered zinc
445 finger transcription factor based on the yeast Gal4 DNA binding domain and viral VP64
446 transactivation domain. The resulting ERK-phosphoGal4v4a transcription factor is able to directly
447 convert ERK kinase activity into up to a 20-fold change in gene expression (**Fig. 3G**). We also
448 show that the sensitivity and specificity of the ERK-phosphoGal4v4a system compares favorably
449 to a classic transcriptional readout, the *FOS* promoter, that is sensitive to many additional signaling
450 cues.

451 The ability to confer kinase-based regulation over target proteins is likely to be widely useful.
452 We have already developed an ERK-controlled Gal4 transcription factor that could be used to
453 measure kinase activity in complex three-dimensional tissues, where resolution can limit the
454 applicability of existing FRET and translocation-based biosensors[53,54], or in cases where high-
455 throughput, non-destructive assays are essential, such as FACS-based isolation of rare cell
456 populations with altered kinase signaling[55]. A kinase-directed transcription factor could also be
457 useful as a synthetic biology tool to trigger novel responses to a cell's signaling state (e.g., by
458 rewiring signaling-hyperactive tumor cells to cytostatic or apoptotic outcomes)[6], or as a method to
459 add feedback loops to intracellular signaling pathways to alter their signal processing[56].

460 This work is only a first step toward a fully generalizable approach in which any kinase could
461 be "wired in" to control any target protein. We have developed an optimized phospho-switch based
462 on the WW phosphorylation-binding domain, but additional binding domains (e.g. FHA1) may be
463 required to broaden the range of kinases and substrates that can be used[57]. Phospho-tyrosine
464 signaling could also be used within a phospho-switch in a similar manner, using the specific
465 interaction between certain phosphotyrosine peptides and SH2 domains[14,58]. Finally, it will be
466 essential to broaden the set of target proteins with potent sites for allosteric control so that a diverse
467 set of cellular outputs will be accessible to novel kinase-based control[15,21,49,51]. These tools and
468 others may help to usher in a new era of kinase-controlled transcriptional responses and synthetic
469 post-translational intracellular logic circuits.

470

471 **Methods**

472 **Plasmid construction**

473 Important plasmids used in this study are listed in Supplementary Table 3. pQC060 was
474 constructed by cloning the wildtype Gal4-VP64 expression cassette from
475 pHR_SFFV_Gal4_VP64_IRES_mCherry (Addgene, #203909) into a PiggyBac backbone. EKAR
476 (88aa hinge version) was amplified from a home-made modified version of pPBJ-EKAR-EV-NES

477 (a gift from University of California-Davis, Albeck lab) with the 116aa hinge shortened to 88aa.
478 pQC061 was constructed by inserting the EKAR amplicon into pQC060 at the Ser22/Lys23
479 allosteric site. pQC171/235 was constructed by inserting and replacing the original AsLOV2
480 insertion with ERK phospho-switch v2/v3 in pHR_SFFV_Actin_optoNB_tagRFP (Addgene,
481 #159595). Phosphorylation site T-to-A mutations were introduced to pQC061 (this study, EKAR-
482 Gal4) via whole backbone PCR using primers containing the target mutation to generate pQC086.
483 Mutations were introduced using the same procedure on 0_001_v2_a1b1c4 (this study, JNK-
484 phosphoGal4v2), pQC256 (this study, JNK-phosphoGal4v3) and pQC171/235 (this study, F-actin
485 ERK-phosphoNanobodies) to generate pQC188, pQC257 and pQC172/pQC236. Other plasmids
486 for cell line generation (this study, pQC131, pQC136 and pQC137) were constructed with a
487 PiggyBac backbone. The no-VP64 control plasmid, pQC238 was constructed by whole backbone
488 PCR to exclude the VP64 in 0_001_v2_a16b1c17 (this study). All plasmids discussed in this
489 section were constructed through In-Fusion assembly (TaKaRa, #638911). All other plasmids not
490 mentioned in this section were generated with Golden Gate Toolkit (QCTK) and will be separately
491 discussed in following sections.

492 **Golden Gate Toolkit (QCTK) Development**

493 Golden Gate Toolkit for fast phospho-switch generation (QCTK) includes Level 0, 1a, 1b and 1c
494 parts (**Fig. 2A**). To generate Level 0 parts, target protein expression vectors were first cloned with
495 desired backbones, promoter sequences and expression markers. For example, a wild type Gal4-
496 VP64 (as target protein) was first cloned into a PiggyBac integration vector with P_{EF1a} as promoter
497 and IRES-mCherry as expression marker. The cloned expression vectors were opened at the
498 allosteric insertion site with BsaI overhangs by PCR amplification. A bacterial EGFP expression
499 cassette (BBa_J72163_P_{GlpT}_sfGFP) was amplified from pYTK001 (Addgene, #65108) with
500 corresponding BsaI overhangs. Digestion with BsaI_HFv2 (New England Biolabs, #R3733S) and
501 ligation with T4 DNA Ligase (New England Biolabs, #M0202S) was then conducted to insert the
502 bacterial EGFP marker into the target protein expression vector and leave BsaI sites on both ends
503 of the EGFP marker. All Level 0 parts are carbenicillin-resistant and successful transformants
504 express EGFP on LB agar plates with carbenicillin (Gold Biotechnology, #C-103-5).

505 To generate Level 1 parts, pYTK001 was amplified as backbones with 1a, 1b or 1c BsmBI
506 overhangs. Desired insert sequences were generated by PCR amplification, oligonucleotide
507 annealing or direct DNA fragment synthesis with corresponding 1a, 1b or 1c BsmBI overhangs.
508 Digestion with BsmBI_v2 (NEB, #R0739S) and ligation with T4 DNA Ligase was conducted to
509 replace the bacterial EGFP marker in pYTK001 with target inserts. All Level 1 parts are
510 chloramphenicol-resistant and successful transformants were picked by EGFP counter-selection
511 on LB agar plates with chloramphenicol (Gold Biotechnology, #C-105-5). Standardized overhang
512 sequences for Level 0, 1a, 1b and 1c parts are shown in **Fig. 2A**. See Supplementary Table 1
513 QCTK1a/c parts) and 2 (QCTK1b parts) for lists of all QCTK parts used in this study.

514 **Variant assembly with QCTK**

515 Golden Gate assembly was performed in a one-pot reaction with Level 0, 1a, 1b and 1c parts.
516 Reaction mixes to assemble variant expression plasmids were prepared individually with all 4 parts
517 (50-100 ng for each part), 0.5 µL BsaI_HFv2, 0.5 µL T4 DNA Ligase, 1 µL T4 DNA Ligase
518 Reaction Buffer (New England Biolabs, #M0202S) to a total volume of 6.5 µL. Reaction mix was
519 incubated for 50x digestion/ligation cycles (2 mins at 37 °C followed by 4 mins at 16 °C).
520 Additional digestion for 10 mins at 37 °C followed by heat inactivation for 10 mins at 80 °C was

521 conducted after the digestion/ligation cycles. Reaction mixes were then transformed into Stellar™
522 Competent Cells (TaKaRa, 636766) and an aliquot of the recovery culture was spread on an LB
523 agar plate with carbenicillin. Successful transformants were picked by counter-selection on EGFP
524 expression (undigested Level 0 part contains the bacterial EGFP expression cassette and
525 undigested Level 1a-c parts are chloramphenicol-resistant). See Supplementary Table 3 for all
526 important plasmids used in this study generated by QCTK Golden Gate assembly.

527 **Cell culture**

528 Lenti-X HEK293T cells and NIH 3T3 cells were maintained in DMEM (Gibco, #11995073) with
529 10% FBS (Fetal Bovine Serum; R&D Systems, #S11150), 1% penicillin/streptomycin (Gibco,
530 #15140-122), 2mM L-Glutamine (Gibco, #25030-081) throughout all experiments. For stem cell
531 cultures, basal growth medium was made with GMEM (Millipore Sigma, G6148), 10% ESC-
532 qualified fetal bovine serum (R&D Systems, S10250), 1×GlutaMAX (Gibco, 35050-061),
533 1×MEM non-essential amino acids (Gibco, 11140-470050), 1 mM sodium pyruvate (Gibco,
534 11360-070), 100 μM 2-mercaptoethanol (Gibco, 47121985-023) and 1% penicillin/streptomycin.
535 Mouse embryonic stem cell (mESC) line, E14tg2a (ATCC, CRL-1821), was maintained in 0.1%
536 gelatin coated 25 cm^2 tissue culture flasks and cultured in 2i+LIF media comprising basal growth
537 medium further supplemented with 1,000 units/ml^{-1} LIF (Millipore Sigma, ESG1107), 2 μM
538 PD0325901 (Tocris, 4192) and 3 μM CHIR (Tocris, 4423). Cells were verified by STR profiling
539 (ATCC). Cells were not cultured in proximity to commonly misidentified cell lines.

540 **Cell transient transfection and ERK stimulation with conditioned media**

541 HEK293T reporter cells were seeded in 48-well plates. 24 hours post seeding, cells were
542 transfected at 60%-80% confluency. Transfection mixtures for each well were prepared in 15 μL
543 Gibco OptiMEM (Gibco, 31985070) containing 2.5 μL FuGENE HD (Promega, #E2311) and
544 150 ng vector plasmid. 24 hours post transfection, culture media was switched to serum-free (SF)
545 media (DMEM with 1% penicillin/streptomycin and 0.00476 mg/mL HEPES (Sigma-Aldrich,
546 H4034)) or fresh growth media (GM, recipe mentioned in Cell culture section). For reactivation,
547 media was replaced with GM at a defined time after first media switch with serum-free media (in
548 **Fig. 1F, 3H**). For delivering multiple pulses of ERK activation with media change, 75% of the
549 existing media in wells were replaced with fresh GM at 6, 18, 24 h after the first media change (0
550 h). All ERK-ON experiments in **Fig. 1H, 2 and 3** were done with 4 GM changes in 30 h. After
551 treatment, cells were then detached with 1 min TrypLE (Gibco, 12604–013) treatment at 37 °C
552 and resuspended into a single-cell solution for flow cytometry analysis. For the hinge variant
553 screen, variants were tested in batches with 3 controls in each batch, including a no-transfection
554 control, a WT-Gal4 control and an ERK-phosphoGal4 variant (0_001_a1b1c1) as reference. Batch
555 correction was done individually for ERK-ON and ERK-OFF conditions using the controls and
556 normalized to the first batch.

557 **Cell line generation**

558 Engineered HEK293T stable cell lines were generated using the piggyBac random integration
559 system. A chassis cell line was first cultured to 60%-80% confluency in 12-well plates.
560 Transfection mixtures were prepared in 45 μl OptiMEM containing 4 μl FuGENE HD, 800 ng
561 vector plasmid and 250 ng PBase 'helper' plasmid (System Biosciences). After preparation, the
562 transfection mixtures were equilibrated at room temperature for 15 min and then added dropwise
563 to the chassis cells. Cultures were propagated for at least four days following transfection. The

564 cells were then detached and resuspended into a single-cell solution for fluorescence-activated cell
565 sorting (FACS) using a Sony SH800S sorter. Sorted fluorescence-positive cells are collected and
566 cultured for experiments.

567 **Flow cytometry analysis and fluorescence-activated cell sorting (FACS)**

568 Flow cytometry analysis or FACS was conducted with a Sony SH800S equipped with Sony
569 100 μm Sorting Chip. Live, single cells were gated using FSC-A and SSC-A (for live cells) and
570 FSC-A and FSC-H (for single cells). EGFP was excited with a 487.5 nm laser, and emitted light
571 was collected after passing through 525/50 nm band pass filters. mCherry was excited with a
572 561 nm laser, and emitted light was collected after passing through 600/60 nm band pass filters.
573 iRFP was excited with a 639 nm laser, and emitted light was collected after passing through
574 720/60 nm band pass filters. Gain configuration and fluorescence compensation was performed
575 following manufacturer instruction. For FACS, at least 100,000 cells were sorted and plated on a
576 new 6-well plate. Detailed strategies of gating, analysis and visualization of flow cytometry data
577 are shown in Fig. S1.

578 **Fold change calculation**

579 Cells were first gated for IRES-mCherry expression level between 5×10^4 to 1.25×10^5 and fold
580 change of the phosphoGal4s were calculated as:

581 $$FC = \frac{TP - ctrl}{AP - ctrl}$$

582 where FC is the fold change reported, TP is the response of phosphoGal4s with phosphorylatable
583 substrate; AP is the response of phosphoGal4s with non-phosphorylatable substrate and ctrl is the
584 response of the control phosphoGal4 lacking VP64.

585 **Multi-variable linear regression model to predict hinge performance**

586 A multi-variable linear regression model was built to use five selected hinge sequence features
587 (length, A%, GS%, EK%, P%) as input variables and output the hinge performance (include
588 maximum activation in ERK-ON condition and background activation in ERK-OFF condition).
589 The model was trained using experimentally tested hinges. Features extracted from experimentally
590 tested hinges were tested negative for multicollinearity with all variance inflation factors (VIF) <
591 5. The trained model was then used to predict the performance of a library of > 6000 *in silico*
592 generated hinge sequences. The library includes GS-rich flexible hinges, EAAAK-repeat alpha
593 helical hinges, AP-repeat proline-rich hinges and computationally random mutated hinges at
594 various lengths. Details of the model are shown in **Fig. S3**.

595 **Optogenetic activation of ERK-phosphoGal4 with optoWELL and flow cytometry**

596 Polyclonal HEK293T cells stably expressing both the optoSOS system and the ERK-
597 phosphoGal4v2/UAS system (**Fig. 4A-B**) were seeded in glass-bottom black 24-well plates
598 (Cellvis, P24-1.5H-N) and kept in dark in the growth media. 24 hours after seeding, culture media
599 was changed to serum-free (SF) media and the plate was then placed on a light-stimulation device
600 (opto biolabs, optoWELL). Each well can be illuminated with 450 nm blue light at a defined
601 intensity and duty cycle profile. Light intensity of the device (in mW/cm^2) is measured with a
602 power meter (Thorlabs, PM100D). After 22 h of stimulation, cells were detached and analyzed
603 with Sony SH800S Cell Sorter. For MEK inhibition experiments, PD 0325901 (Tocris, 4192) was

604 diluted in serum-free media at a final concentration of 10 μM and cells were kept in PD 0325901-
605 contaning serum-free media throughout 22 h of stimulation. To supplement the system with zinc,
606 additional $ZnCl_2$ (Sigma-Aldrich, 208086) was added to the serum-free media.

607 **Signaling pathway stimulation**

608 Polyclonal HEK293T cell lines harboring P_{FOS}-dEGFP or ERK-phosphoGal4v4/UAS-dEGFP
609 reporting system were seeded in 48 well plates. 24 h after seeding, cells were incubated in 200 uL
610 serum-free (SF) media overnight (~18 hrs.). After overnight starvation, drugs used for various
611 stimulation are pre-diluted in serum-free media in 2x concentration. 100 uL previously in-well
612 media was removed and replaced with 2x stimulation media. 4 h after stimulation, cells were
613 detached and analyzed with Sony SH800S Cell Sorter. Following drugs were used in the panels:
614 PMA (Phorbol 12-myristate 13-acetate; Sigma-Aldrich, P8139), ionomycin (Sigma-Aldrich,
615 407950), forskolin (Calbiochem, 34-428-25MG) and anisomycin (Sigma-Aldrich, A9789).

616 **Dose-response curve fitting**

617 Dose-response curve in Fig. 4E/5B was fitted with a four-parameter logistic (4PL) model. The
618 model was defined as:

619 $$y = D + \frac{A - D}{1 + (\frac{x}{EC50})^S}$$

620 where D is the maximum response, A is the minimum response, EC50 is the half-maximal effective
621 concentration and S is Hill's slope of the curve. The concentration or intensity of the input and the
622 mean response were used to fit the model.

623 **Live-cell imaging**

624 Cells were kept at 37 ˚C with 5% CO_2 for the duration of all imaging experiments. 50 μL of mineral
625 oil was pipetted onto the wells right before placing onto the scope to prevent media from
626 evaporating. Imaging was done using Nikon Eclipse Ti microscope with a Prior linear motorized
627 stage, a Yokogawa CSU-X1 spinning disk, an Agilent laser line module containing 405, 488, 561
628 and 650 nm lasers, an iXon DU897 EMCCD camera and objective lenses as specified for
629 individual experiments in the following sections.

630 **Optogenetic activation of ERK-phosphoGal4 with live-cell imaging**

631 Polyclonal engineered HEK293T cells stably expressing both the optoSOS system and the ERK-
632 phosphoGal4v2/UAS system (**Fig. 4A-B**) were seeded in glass-bottom black 96-well plates
633 (Cellvis, P96-1.5H-N) and kept in dark in the growth media. 24 h after seeding, culture media was
634 changed to serum-free (SF) media and the cells were kept in starvation and in dark for ~24 h to
635 ensure low baseline EGFP before imaging and stimulation on microscope. Cells were then imaged
636 with previous specified microscope configuration with a 20x air objective lens. A 450 nm LED
637 light source was used for photoexcitation with blue light, which was delivered through a
638 Polygon400 digital micro-mirror device (DMD, Mightex Systems). The LED power was adjusted
639 to 75% to deliver ~15 mW/cm^2 blue light at the sample plane, as measured by with a PM100D
640 power meter (Thorlabs). Light was delivered as 1 s pulses of illumination every 1.5 mins
641 throughout 17 h of imaging. ErkKTR-iRFP was captured every 3 mins, EGFP induction and IRES-
642 mCherry expression were captured every 1 h throughout the entire imaging session.

643 For ErkKTR quantification in this experiment, cells were segmented on whole cell fluorescence
644 in the mCherry channel using Cellpose3[59]. tagBFP, EGFP, mCherry and iRFP signal can be
645 measured inside individual cell masks. Inside the segmented mask for an individual cell, the
646 tagBFP signal was thresholded to generate a cytosolic region mask due to the natural cytosolic
647 localization of the tagBFP-SSPB-SOScat protein. Whole cell masks can then be further divided
648 into cytosolic masks and nucleus masks. ErkKTR-iRFP intensity was measured separately in both
649 regions for each cell.

650 **Live-cell imaging for the F-actin ERK-phosphoNanobody**

651 Monoclonal HEK293T cells expressing NLS-tagBFP and ErkKTR-iRFP were seeded at low cell
652 density in fibronectin-coated 96 well glass-bottom plates (fibronectin coating concentration, 5
653 μg/cm^2). 24 h after seeding, cells were transfected with F-actin ERK-phosphoNanobody
654 expression plasmids using FuGENE HD (same procedure as previously described transfections).
655 24 h after transfection, cells were starved overnight (>12 hours) with serum-free media and then
656 imaged with previous specified microscope configuration with a 60x oil immersion objective lens.
657 For MEK inhibition conditions, cells were pre-treated with U0126 (catalog) at a final concentration
658 of 10 μM for at least 30 mins prior serum stimulation. To apply the MEK inhibitor, 1 μL 10 mM
659 U0126 stock was pre-diluted in 19 μL serum-free media and 2 μL from the dilution was added in
660 wells with a total media volume of 100 μL at least 30 mins before imaging. Images of iRFP (on
661 ErkKTR) and tagRFP (on F-actin ERK-phosphoNanobody) were taken every 30 s for >20 mins.
662 2.5 mins after the start of imaging, 2.5 μL of FBS was added directly into wells to activate ERK
663 signaling.

664 **Competing interests**

665 J.E.T. is a scientific advisor for Prolific Machines and Nereid Therapeutics. The authors have
666 also submitted a provisional patent application related to kinase-controlled protein switches. The
667 remaining authors declare no conflicts of interest.

668 **Author Contributions**

669 Conceptualization, Q.C., J.E.T.; Methodology, Q.C., J.E.T.; Investigation, Q.C.; Funding,
670 J.E.T.; Writing and Editing, Q.C., J.E.T.; Supervision, J.E.T.

671 **Acknowledgements**

672 We thank all members of the Toettcher lab for helpful discussions and Beatrice Ramm, Emily
673 Kolenbrander Ho, and Long Nguyen for comments on the manuscript. This work was supported
674 by the National Institutes of Health grant R01GM144362 and NSF RECODE grant 2134935 (to
675 J.E.T.).

676

References

1. Venta, R. *et al.* A processive phosphorylation circuit with multiple kinase inputs and mutually diversional routes controls G1/S decision. *Nat Commun* **11**, 1836 (2020).

2. Huang, C. Y. & Ferrell, J. E. Ultrasensitivity in the mitogen-activated protein kinase cascade. *PNAS* **93**, 10078–10083 (1996).

3. Barkai, N. & Leibler, S. Robustness in simple biochemical networks. *Nature* **387**, 913–917 (1997).

4. Elowitz, M. B. & Leibler, S. A synthetic oscillatory network of transcriptional regulators. *Nature* **403**, 335–338 (2000).

5. Gardner, T. S., Cantor, C. R. & Collins, J. J. Construction of a genetic toggle switch in Escherichia coli. *Nature* **403**, 339–342 (2000).

6. Chung, H. K. *et al.* A compact synthetic pathway rewires cancer signaling to therapeutic effector release. *Science* **364**, eaat6982 (2019).

7. Chen, Z. *et al.* A synthetic protein-level neural network in mammalian cells. *Science* **386**, 1243–1250 (2024).

8. Samaniego, C. C., Moorman, A., Giordano, G. & Franco, E. Signaling-based neural networks for cellular computation. in *2021 American Control Conference (ACC)* 1883–1890 (2021). doi:10.23919/ACC50511.2021.9482800.

9. Daniels, K. G. *et al.* Decoding CAR T cell phenotype using combinatorial signaling motif libraries and machine learning. *Science* **378**, 1194–1200 (2022).

10. Chen, Z. & Elowitz, M. B. Programmable protein circuit design. *Cell* **184**, 2284–2301 (2021).

11. Gao, X. J., Chong, L. S., Kim, M. S. & Elowitz, M. B. Programmable protein circuits in living cells. *Science* **361**, 1252–1258 (2018).

12. Pincus, D. *et al.* Engineering allosteric regulation in protein kinases. *Science Signaling* **11**, eaar3250 (2018).

13. Gordley, R. M. *et al.* Engineering dynamical control of cell fate switching using synthetic phospho-regulons. *Proc Natl Acad Sci U S A* **113**, 13528–13533 (2016).

14. Yang, X. *et al.* Engineering synthetic phosphorylation signaling networks in human cells. *Science* **387**, 74–81 (2025).

15. Dagliyan, O. *et al.* Engineering extrinsic disorder to control protein activity in living cells. *Science* **354**, 1441–1444 (2016).

16. Dagliyan, O. *et al.* Rational design of a ligand-controlled protein conformational switch. *Proceedings of the National Academy of Sciences* **110**, 6800–6804 (2013).

17. Harvey, C. D. *et al.* A genetically encoded fluorescent sensor of ERK activity. *PNAS* **105**, 19264–19269 (2008).

18. Komatsu, N. *et al.* Development of an optimized backbone of FRET biosensors for kinases and GTPases. *Mol. Biol. Cell* **22**, 4647–4656 (2011).

715 19. Newman, R. H., Fosbrink, M. D. & Zhang, J. Genetically Encodable Fluorescent Biosensors
716 for Tracking Signaling Dynamics in Living Cells. *Chem. Rev.* **111**, 3614–3666 (2011).

717 20. Greenwald, E. C., Mehta, S. & Zhang, J. Genetically Encoded Fluorescent Biosensors
718 Illuminate the Spatiotemporal Regulation of Signaling Networks. *Chem Rev* **118**, 11707–11794
719 (2018).

720 21. Zhu, L., McNamara, H. M. & Toettcher, J. E. Light-switchable transcription factors obtained
721 by direct screening in mammalian cells. *Nat Commun* **14**, 3185 (2023).

722 22. Goglia, A. G. *et al.* A Live-Cell Screen for Altered Erk Dynamics Reveals Principles of
723 Proliferative Control. *Cell Syst* **10**, 240-253 e6 (2020).

724 23. Albeck, J. G., Mills, G. B. & Brugge, J. S. Frequency-modulated pulses of ERK activity
725 transmit quantitative proliferation signals. *Molecular cell* **49**, 249–61 (2013).

726 24. Aoki, K. *et al.* Stochastic ERK activation induced by noise and cell-to-cell propagation
727 regulates cell density-dependent proliferation. *Molecular cell* **52**, 529–40 (2013).

728 25. Regot, S., Hughey, J. J., Bajar, B. T., Carrasco, S. & Covert, M. W. High-Sensitivity
729 Measurements of Multiple Kinase Activities in Live Single Cells. *Cell* **157**, 1724–1734 (2014).

730 26. Abramson, J. *et al.* Accurate structure prediction of biomolecular interactions with AlphaFold
731 3. *Nature* **630**, 493–500 (2024).

732 27. Macias, M. J. *et al.* Structure of the WW domain of a kinase-associated protein complexed
733 with a proline-rich peptide. *Nature* **382**, 646–649 (1996).

734 28. Kato, Y., Ito, M., Kawai, K., Nagata, K. & Tanokura, M. Determinants of Ligand Specificity
735 in Groups I and IV WW Domains as Studied by Surface Plasmon Resonance and Model
736 Building *. *Journal of Biological Chemistry* **277**, 10173–10177 (2002).

737 29. Kato, Y. *et al.* Common Mechanism of Ligand Recognition by Group II/III WW Domains:
738 REDEFINING THEIR FUNCTIONAL CLASSIFICATION *. *Journal of Biological Chemistry*
739 **279**, 31833–31841 (2004).

740 30. Toettcher, J. E., Weiner, O. D. & Lim, W. A. Using optogenetics to interrogate the dynamic
741 control of signal transmission by the Ras/Erk module. *Cell* **155**, 1422–34 (2013).

742 31. Johnson, H. E. *et al.* The Spatiotemporal Limits of Developmental Erk Signaling.
743 *Developmental Cell* **40**, 185–192 (2017).

744 32. Guntas, G. *et al.* Engineering an improved light-induced dimer (iLID) for controlling the
745 localization and activity of signaling proteins. *PNAS* **112**, 112–117 (2015).

746 33. Hong, M. *et al.* Structural Basis for Dimerization in DNA Recognition by Gal4. *Structure* **16**,
747 1019–1026 (2008).

748 34. Glassman, A. B., Rydzewski, R. S. & Bennett, C. E. Trace metal levels in commercially
749 prepared tissue culture media. *Tissue and Cell* **12**, 613–617 (1980).

750 35. Lo, M. N., Damon, L. J., Wei Tay, J., Jia, S. & Palmer, A. E. Single cell analysis reveals
751 multiple requirements for zinc in the mammalian cell cycle. *eLife* **9**, e51107 (2020).

752 36. McNamara, H. M., Solley, S. C., Adamson, B., Chan, M. M. & Toettcher, J. E. Recording
753 morphogen signals reveals mechanisms underlying gastruloid symmetry breaking. *Nat Cell Biol*
754 1–13 (2024) doi:10.1038/s41556-024-01521-9.

755 37. Inglés-Prieto, Á. *et al.* Light-assisted small-molecule screening against protein kinases. *Nat*
756 *Chem Biol* **11**, 952–954 (2015).

757 38. Durick, K. & Negulescu, P. Cellular biosensors for drug discovery. *Biosensors and*
758 *Bioelectronics* **16**, 587–592 (2001).

759 39. Serup, P. *et al.* Partial promoter substitutions generating transcriptional sentinels of diverse
760 signaling pathways in embryonic stem cells and mice. *Disease Models & Mechanisms* **5**, 956–
761 966 (2012).

762 40. Joo, J.-Y., Schaukowitch, K., Farbiak, L., Kilaru, G. & Kim, T.-K. Stimulus-specific
763 combinatorial functionality of neuronal c-fos enhancers. *Nat Neurosci* **19**, 75–83 (2016).

764 41. Morgani, S. M. *et al.* A Sprouty4 reporter to monitor FGF/ERK signaling activity in ESCs
765 and mice. *Developmental Biology* **441**, 104–126 (2018).

766 42. Ravindran, P. T., McFann, S., Thornton, R. H. & Toettcher, J. E. A synthetic gene circuit for
767 imaging-free detection of signaling pulses. *Cell Systems* **13**, 131-142.e13 (2022).

768 43. MacKeigan, J. P., Murphy, L. O., Dimitri, C. A. & Blenis, J. Graded Mitogen-Activated
769 Protein Kinase Activity Precedes Switch-Like c-Fos Induction in Mammalian Cells. *Mol Cell*
770 *Biol* **25**, 4676–4682 (2005).

771 44. Herschman, H. R. PRIMARY RESPONSE GENES INDUCED BY GROWTH FACTORS
772 AND TUMOR PROMOTERS. *Annual Review of Biochemistry* **60**, 281–319 (1991).

773 45. Janknecht, R., Cahill, M. A. & Nordheim, A. Signal integration at the c-fos promoter.
774 *Carcinogenesis* **16**, 443–450 (1995).

775 46. Calcium regulation of gene expression in neuronal cells - Ghosh - 1994 - Journal of
776 Neurobiology - Wiley Online Library.
777 https://onlinelibrary.wiley.com/doi/abs/10.1002/neu.480250309.

778 47. Chung, L. A Brief Introduction to the Transduction of Neural Activity into Fos Signal. *Dev*
779 *Reprod* **19**, 61–67 (2015).

780 48. Yusa, K., Zhou, L., Li, M. A., Bradley, A. & Craig, N. L. A hyperactive piggyBac transposase
781 for mammalian applications. *Proc Natl Acad Sci U S A* **108**, 1531–6 (2011).

782 49. Gil, A. A. *et al.* Optogenetic control of protein binding using light-switchable nanobodies.
783 *Nat Commun* **11**, 4044 (2020).

784 50. Karginov, A. V., Ding, F., Kota, P., Dokholyan, N. V. & Hahn, K. M. Engineered allosteric
785 activation of kinases in living cells. *Nat Biotech* **28**, 743–747 (2010).

786 51. Reynolds, K. A., McLaughlin, R. N. & Ranganathan, R. Hot Spots for Allosteric Regulation
787 on Protein Surfaces. *Cell* **147**, 1564–1575 (2011).

788 52. Carrasco-Lopez, C. *et al.* Development of light-responsive protein binding in the monobody
789 non-immunoglobulin scaffold. *Nat Commun* **11**, 4045 (2020).

790 53. Zhao, M., Wan, X., Li, Y., Zhou, W. & Peng, L. Multiplexed 3D FRET imaging in deep tissue
791 of live embryos. *Sci Rep* **5**, 13991 (2015).

792 54. Hirata, E. & Kiyokawa, E. Future Perspective of Single-Molecule FRET Biosensors and
793 Intravital FRET Microscopy. *Biophysical Journal* **111**, 1103–1111 (2016).

794 55. Gerosa, L. *et al.* Receptor-Driven ERK Pulses Reconfigure MAPK Signaling and Enable
795 Persistence of Drug-Adapted BRAF-Mutant Melanoma Cells. *Cell Systems* **11**, 478-494.e9
796 (2020).

797 56. Mitchell, A., Wei, P. & Lim, W. A. Oscillatory stress stimulation uncovers an Achilles' heel
798 of the yeast MAPK signaling network. *Science* **350**, 1379–83 (2015).

799 57. Gao, X. & Zhang, J. Spatiotemporal Analysis of Differential Akt Regulation in Plasma
800 Membrane Microdomains. *MBoC* **19**, 4366–4373 (2008).

801 58. Farahani, P. E. *et al.* pYtags enable spatiotemporal measurements of receptor tyrosine kinase
802 signaling in living cells. *eLife* **12**, e82863 (2023).

803 59. Stringer, C. & Pachitariu, M. Cellpose3: one-click image restoration for improved cellular
804 segmentation. *Nat Methods* **22**, 592–599 (2025).

805